Chemosphere 257 (2020) 127237

Contents lists available at ScienceDirect

Chemosphere

journal homepage: www.elsevier.com/locate/chemosphere

Real-time monitoring of toxic components from fine dust air pollutant samples by utilizing spark-induced plasma spectroscopy

Jun-Ho Yang [a], Jaehun Jung [b], Ji-Hoon Ryu [a], Jack J. Yoh [a, *]

[a] Department of Mechanical & Aerospace Engineering, Seoul National University, Republic of Korea
[b] Department of Aerospace System Engineering, Seoul National University 1 Gwanakro, Gwanakgu, Seoul, 151-742, Republic of Korea

HIGHLIGHTS

- SIPS device for quantitative monitoring of airborne toxic pollutants was developed.
- Proposed sensing device can be utilized for measuring airborne toxic pollutants.
- Concentrations of heavy metals and ammonia were differentiated as small as 0.1 μg/m^3.
- Overall detection limit showed a five-fold enhancement over LIPS.

ARTICLE INFO

Article history:
Received 24 February 2020
Received in revised form
24 May 2020
Accepted 26 May 2020
Available online 1 June 2020

Handling Editor: R Ebinghaus

Keywords:
Fine dust
Air pollutant
Spark-induced plasma spectroscopy (SIPS)
Heavy metals
Ammonia
Plasma emissions

ABSTRACT

A growing modern-day concern is fine dust air pollution that contains heavy metals and ammonium ions (NH_4^+) from industrial and agricultural waste sources, respectively. In the current study, the development of an innovative and effective technique for real-time, quantitative monitoring of toxic fine dust components using plasma emission spectroscopy is presented as a complement to emergency preparedness plans aimed at reducing dust pollution. A novel spark-induced plasma spectroscopic (SIPS) device that can control the frequency and magnitude of plasma was developed for the toxic pollutants in this work. SIPS utilizes an electrical discharge from a high voltage at a low current to produce plasma when the applied voltage is higher than the ambient voltage surrounding the electrodes. The detection limit of this setup was enhanced by a factor of 4.3 over laser-induced plasma spectroscopy (LIPS). This compact sensing device was used in combination with a new quantitative analytical method to measure the concentration of heavy metals and ammonia molecules in fine dust air pollution. By integrating the time-resolved plasma emission signals that were based on the plasma continuum decay time of each element, quantitative measurements of the minute changes in composition of 0.1 μg/m^3 were conducted. The findings of this study could inspire future research on the use of SIPS for monitoring airborne fine dust pollutants with better sensitivity in real-time *via* a new quantitative analytical method.

1. Introduction

Fine dust pollution is a big concern globally due to the high demands of the modern lifestyle. The air quality, specifically around developed sections and urban centers, is affected by the particulate matter (PM) concentration. Fine dust was recognized by the World Health Organization (WHO) as a first-class carcinogen in 2013 following the devastating smog that developed in China earlier that year (Lelieveld et al., 2015; Park et al., 2018). Dust refers to PM that is floating or scattered in the air, whereas fine dust refers to extremely small dust particles. Particulates with a diameter of 10 μm or less are classified as PM 10, whereas those with a diameter of 2.5 μm or less are categorized as PM 2.5 (Ehrlich et al., 2007; Prospero et al., 2001).

Fine dust contains substances that pose a severe threat to human health. Ammonia produced in agricultural complexes, nitrogen oxides present in vehicle exhaust gases, and sulfur oxides produced in industrial complexes are all well-known toxic compounds. Also, heavy metals may be present in fine dust dispersions. Altogether, these substances can cause a multitude of diseases, and the worst-case scenario may lead to death (Choi et al., 2018; Dastoorpoor et al., 2018; Dianat et al., 2016). Owing to these adverse

* Corresponding author.
E-mail address: jjyoh@snu.ac.kr (J.J. Yoh).

https://doi.org/10.1016/j.chemosphere.2020.127237
0045-6535/

health effects, heavy metals and toxic gases in fine dust have been extensively studied in the past (Abdel-Latif and Saleh., 2012; Cho et al., 2018; Hadei and Naddafi, 2020; Guo et al., 2002; Neisi et al., 2017; Ng et al., 2003; Park et al., 2018). Therefore, for characterizing the generation and migration of these toxic substance, the two primary studies on such PM dust categories have been recently reported as (1) a collection of PM from cities to investigate their chemical properties over time (Winchester, 1981; N. Sugimoto et al., 2003; Zhang et al., 2013a, 2013b; Yu et al., 2011; Stone et al., 2011; VanCuren and Cahill, 2002; Cyrys et al., 2003) and (2) a simulation of certain situations from the agricultural or industrial settings where high quantities of sulfur oxides, ammonia, and ammonium are produced (Zhang et al., 2013a, 2013b; Hagen, 2004). In the previous research (Winchester, 1981; N. Sugimoto et al., 2003; Zhang et al., 2013a, 2013b; Yu et al., 2011; Stone et al., 2011; VanCuren and Cahill, 2002; Cyrys et al., 2003; Zhang et al., 2013a, 2013b; Hagen, 2004), changes in the fine dust components at particular pollution sites and in certain real-world situations were investigated. These studies helped us to identify the origin of the fine dust particulates and implement effective countermeasures such as a real-time alert system based on real-time analysis of the fine dust dispersion patterns in highly populated cities.

Plasma spectroscopy is an atomic emission spectroscopic technique used in multi-elemental analyses. The laser-induced plasma spectroscopy (LIPS) is a representative spectroscopic technique that was previously applied to dust monitoring. In particular, the present study focuses on the spark-induced plasma spectroscopy (SIPS) as opposed to LIPS, favorably owing to its recently discovered advantages for both real-time analysis and easy integration into the compact mobile devices. SIPS was first introduced in 2000 to measure the concentration of heavy metals in plasma emissions (Hunter et al., 2000a, 2000b). Since then, the spark-induced breakdown effect has been used as a supplement to LIPS or laser ablation to improve the signal intensity of the plasma emissions (Vieira et al., 2018; He et al., 2018; Srungaram et al., 2013). In addition to the improved cost-effectiveness of SIPS, it can be configured and manufactured into a relatively compact size when compared to LIPS. Moreover, SIPS is useful for analyzing gaseous dispersions in situations where the breakdown voltage of the medium is relatively low. SIPS is also known for having a superior limit of detection (LOD) when compared with LIPS in the gas phase (Jung et al., 2020). Similar to this study, Khalaji et al. (2012) used SIPS for dust monitoring in which the atomic signals, such as those for calcium and magnesium, were measured according to particle size. The application of SIPS in a real-world experimental environment was demonstrated through Hunter's work on airborne heavy metals in aerosols and the subsequent detection of chromium and lead signals (Hunter et al., 2000a, 2000b). In a report by Kammermann et al. (2018), a study was conducted to detect the methane/air ratio in engine emissions using SIPS. Yao et al. (2018) prepared samples in which the concentrations of C, MgO, and SiO_2 in flowing particles were varied, and the subsequent quantitative analysis of the carbon components was performed using SIPS. Through these examples, we can see that SIPS is recognized as a suitable analytical technique for gases.

In the present work, an innovative SIPS device that can control the magnitude and frequency of plasma *via* a customized micro control unit (MCU) was designed to be adaptable to the unstable atmospheric conditions that cause variances in the plasma generation process. Compared with other conventional camera−spectrometer setups, the present system was configured to be compact as it used only a few components, namely a band-pass filter and photodiode. In addition to this novel system configuration, a new quantitative analytical or chemometric method was developed by integrating the photodiode signals in a time-resolved format that uses the optimal detection of the spark-induced plasma emissions. Two experiments were conducted to verify the suitability of the detection device: (1) detecting the change of the total concentration of fine dust, and (2) measuring of the concentration of specific components in the same fine dust sample. The total concentration of fine dust was reflected by the magnitude of the electrical signal, whereas changes in the concentration of the specific component were measured by integrating the electrical signals.

In short, the objectives of this work can be expressed as follows: 1) to configure the SIPS to control the plasma size and its generation frequency for fine dust analysis, 2) set up a small-scale sensing system for quantitative chemical analysis, and 3) conduct real-time monitoring of heavy metals and ammonia.

2. Materials and methods

2.1. Sample preparation

Fine dust samples were collected using PM 10 and PM 2.5 cyclone filter pack systems (ParticleSampler C, Sant Inc.) at a flow rate of approximately 17 L/min. The filter that was 47 mm in diameter, was composed of a PTFE membrane and quartz filter with a pore size of 2.0 μm.

Multiple devices were utilized to simulate windy conditions that contain fine dust dispersions (Fig. 1(a) and (b)). A chamber ($100 \times 100 \times 100\ cm^3$) in which a fan circulated air at the flow rate of 100−200 m^3/h was designed to prevent external airflow and made from transparent acrylic to minimize any difficulty associated with measuring plasma light from the outside. The fine dust sample was collected from Seoul, where 3.3 g of suitable dust sample was extracted over ten days for use in ICP−MS and ion chromatography.

For quantification and qualification purposes, ICP−MS (NexION 350D, PerkinElmer) and MC−ICP−MS (Nu Instruments, UK) methods combined with a laser ablation system were used to detect the metal concentrations in the fine dust samples. An ion chromatography method, GC−HRMS (gas chromatography−high-resolution mass spectrometer, JWL-700, Japan), was used to detect the concentration of the ion component in the samples. Quantification of the fine dust samples was performed using the ion and metal concentrations detected through these data as references. The concentration of the ions and metals detected are presented in Table S1.

2.2. Spark-induced plasma (SIP)

While laser system is not quite extreme environment friendly due to its bulky size and low electrical efficiency, SIPS can produce a higher concentration of plasma in the gaseous state when compared with the LIPS (Jung et al., 2020). The SIPS technique operates by first discharging a spark via electrical charging under the high voltage. The discharge occurs when the voltage is higher than the breakdown voltage of the medium around the electrodes, which in turn generates the plasma. Following the plasma generation, the information on the atomic components of the fine dust dispersion is readily obtained as the excited electrons of the atoms return to their lowest energy state.

The SIPS schematic is presented in Fig. 1(b) for the production of a spark *via* a high voltage discharge. The circuit for the spark-induced plasma consisted of a power supply (UltraVolt 6C24−P30, 6 kV, 90 mA) that provided a high DC voltage, a parallel coupling of two high-voltage capacitors (HVCAP DMS HV Capacitor, 0.1 μF, 30000 Vdc) to store electricity, a charging resistor with a gap switch, diodes, and an electrical converter that facilitated conversion from AC to DC. The spark-induced plasma was generated from a tungsten electrode

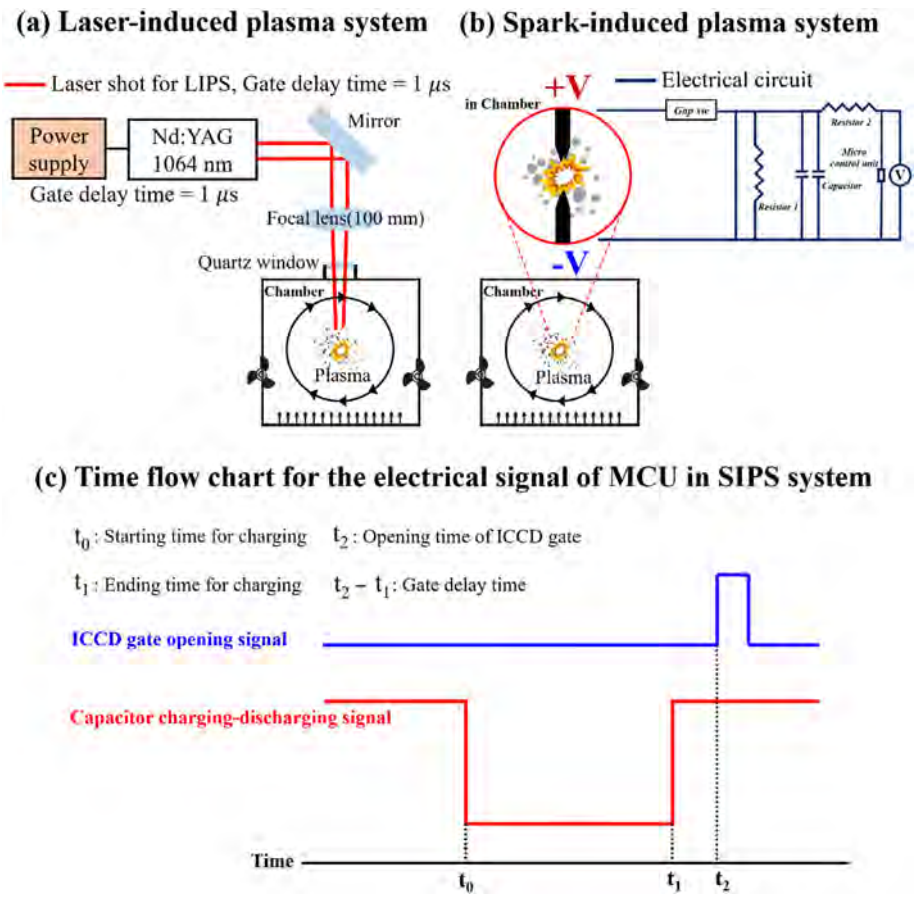

Fig. 1. Systems for producing (a) laser-induced and (b) spark-induced plasmas. (c) Time flow chart for the electrical signal using MCU in the SIPS system.

pair with a purity of ≥99.7%. A micro control unit (Arduino Uno R3) was used to connect with the ICCD system and to control the size and frequency of the plasma. Fig. 1(c) shows how the gate "on/off" of the ICCD camera is controlled using the MCU by transmitting an electrical signal after the capacitor charging time had passed. Typically, the optimal gate delay ($t_2 - t_1$) is set up using the laser-induced plasma measurement method. In our case, the MCU was designed to signal for the generation of a spark instead of a laser, as is standard for a conventional gate generator. Furthermore, the MCU could control the generating time and magnitude of the plasma.

2.3. Laser-induced plasma (LIP)

The LIPS experimental setup is presented in Fig. 1(a). The 1064-nm wavelength Q-switched Nd:YAG laser (Surelite II, Continuum Inc.) was used to make the laser-induced plasma. The pulse duration was set to 5 ns. A pulse generator (BNC 565-8CG) and an oscilloscope (Tektronix TDS-2014) were utilized to synchronize with the spectrometer that was coupled with the ICCD camera. Furthermore, to capture plasma emissions, an optic collector and fiber were used to send the plasma emission signal to the spectrometer (Mechelle 5000, Andor) coupled with the ICCD camera (iStar, Andor). The gate delay time of the ICCD was set to 1 μs, and the gate width was fixed at 20 μs. In this study, the LIPS data was used to compare the precision of the SIPS signals.

2.4. Sensing device for plasma emissions using the photodiode and band-pass filter

The proposed device was designed to produce electrical signals upon the detection of heavy metals and ammonia in fine dust samples without the need for a bulky spectrometer and the ICCD configuration. Previously, the capacity of photodetectors for use in combustion and flame diagnostics was established, and their performance was compared with the performance of spectrometers (Jun et al., 2018). The previous setup was aimed at finding the equivalence ratio by detecting the oxygen and hydrogen signals emitted in a flame. For measuring the concentration of heavy metals and ammonia in fine dust air samples, the setup was also compactly designed to be ideal for mobile and field applications, thus facilitating real-time quantitative analysis.

Here, two lens tubes (SM05V05, Thorlabs) were equipped in the sensing device and were sealed in the tubes. The length of the lens tubes was 26.2 mm, and diameter was 17.8 mm. Since the other components were fixed inside, the size of these two lenses determined the total size of the measuring unit. The atomic and molecular lines for plasma emission of Pb, Fe, Cu, and NH exhibited a strong correlation with the concentrations of heavy metals and ammonia. Thus, the sensing device included four band-pass filters for the atomic lines of Pb (405.78 nm), Fe (238.20 nm), Cu (324.75, 327.39, and 521.82 nm), and NH fluorescence (336 nm). Fig. 2(a) presents a schematic of the proposed simple setup in comparison to a conventional ICCD setup shown in Fig. 2(b). Band-pass filters for Pb detection (405FS10−12.5, Andover) with a center wavelength (CWL) of 405 nm and for Fe detection (280FS10−12.5, Andover) with a CWL of 280 nm were utilized to target Pb and Fe signals, respectively. Additionally, the full width at half maximum (FWHM) was set to 10 nm. For the Cu and NH signals, three different band-pass filters (326FS10−12.5, 520FS10−12.5, 337FS03−12.5, Andover) were used. All of these filters were

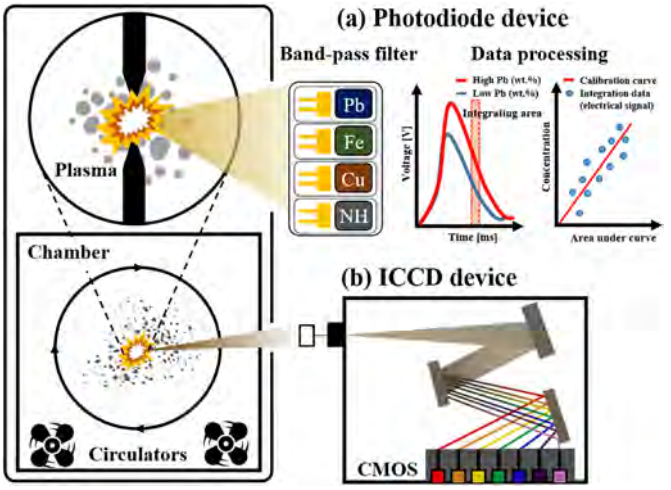

Fig. 2. Comparison between (a) simple photodiode detector and (b) conventional spectrometer (ICCD).

12.5 mm in diameter. We installed Si photodiodes (FDS010, Thorlabs) in the measuring unit to capture plasma emissions. The rise time for the photodiode was 1 ns, and peak responsivity was 0.44 A/W at 238 nm. The four different photodiodes were connected *via* an oscilloscope (Tektronix TDS-2014) equipped with BNC cables to capture the electrical signals in real-time.

3. Results and discussion

3.1. Comparison between SIP and LIP in air

The LIPS and SIPS signals for pure air (dust-free) samples were compared. Here, such pure air state is defined when the concentration of fine dust is 3 $\mu g/m^3$or less. For LIPS, the laser energy was fixed at 40 mJ, and the 30 spectra obtained were averaged for all experiments. SIPS used the total electrical energy of 2 J to generate a spark. In the pure air without any fine dust, LIP and SIP did not exhibit much difference in the amount of nitrogen and oxygen present. However, the signal intensity of SIPS was 3–4 times greater than the signal intensity of LIPS. The signals observed at 744, 746, and 868 nm were assigned to N I, whereas the signal at 777 nm was assigned to O II. The main emission lines from samples with fine dust air pollution samples are presented in Table S2.

Fig. 3(a) and (b) present a comparison of the emission spectra for laser-induced and spark-induced plasmas in dust-free Air. For laser-induced plasma, the signal of the plasma emission light increased when the laser energy was increased. This observation was attributed to the influence exerted by the more efficient heat transfer processes commonly observed in LIPS. A similar trend was observed for SIPS in that the signal intensity increased as the gap distance between the electrodes widened up to a certain distance. Additionally, as the electrode gap increased, the breakdown medium increased, thereby increasing the amount of voltage required. Thus, larger electrode gaps resulted in increased breakdown due to the high voltage discharge that was excited by the plasma. This was confirmation that an expansion in the electrode gap had the same effect as the increase in the laser energy of the system.

If the plasma emission light equation is used as an example, we see that higher voltages lead to a temperature rise and higher total amount of the material excited. A knock-on effect of this is the increase in the plasma emission light signal due to the widening of the electrode gap. In this study, the optimal SIPS setup for detecting the plasma emission light was set to 5 mm. When the electrode gap was larger than 5–6 mm, an arc was generated instead of a spark, and continuous electric discharge occurred. Since the plasma must be selectively generated at the desired time, electrical discharge *via* a spark was preferred. Thus, all experiments were conducted with an electrode gap distance of 5 mm to eliminate the risk of generating an arc. Using Eqn. (1), it was verified that the electrode gap distance enhanced the total amount of atomic density in the plasma, thereby facilitating more efficient heat transfer processes.

$$I = FN_a^I A_{ul} \frac{g_u}{U_a^I} \exp\left(\frac{-E_u}{K_B T}\right) \quad (1)$$

Herein, I is the signal intensity of plasma emission, F is the experimental parameter, N_α^I is the number density of the species at various ionization stages, A_{ul} is the atomic number density indicating the transition probability, g_u is the upper-level degeneracy, and U_α^I is the partition function of temperature, T.

Pellet samples containing inert binders in calcite were prepared to determine the effectiveness of SIPS, and the plasma spectroscopy was quantitatively conducted. The total energy of 2 J was used for SIPS experiments, whereas LIPS experiments utilized 40 mJ of laser energy. However, the electrical energy for the laser system was expected to be higher than 2 J in the LIPS system. Theoretically, the electrical voltage required to generate the plasma was high due to the high voltage for SIPS, but in practice, the entire operation was possible with the commonly used 220 V capacity power supply.

As seen in Fig. 3(c), calcium and carbon signals were detected in both SIPS and LIPS using a 100% calcite mass. As the proportion of calcite decreased, the intensities of the calcium signals for both LIPS and SIPS decreased, and the signal change was constant (Fig. 3(d)). For SIPS, the Ca II signal (393 nm) varied from approximately 8,000 to 3,000, whereas the signal intensity varied from 4,500 to 1,000 for LIPS. When analyzing the gaseous state, the SIPS signal strength was three times greater; however, solid samples exhibited an improvement in signal strength that was approximately two times lower than that seen in the gaseous state. This was because the breakdown medium in the solid sample was lower than that observed in the gas state, thereby causing an increase in the electrical resistance. Consequently, the efficacy of the SIPS method could be confirmed by tracing the calcium signal obtained from the quantitative analysis of calcite. Herein, the LOD was lower in comparison to the results obtained from the LIPS analysis. This meant that gaseous samples could also be used in this study. In analytical chemistry and spectroscopic studies, the LOD generally indicates the lowest quantity of a substance that can be detected. The LOD can be calculated using Eq. (2), where S is the correlation between mass concentration and signal intensity derived from the slope of quantitative analysis, and σ_b is the standard deviation obtained from the quantitative experiments. The LOD of the SIPS and LIPS methods were 19 and 82 ppm, respectively, which corresponds to a 4.3 times enhancement.

$$LOD = \frac{3\sigma_b}{S} \quad (2)$$

3.2. Particle size effect

Fig. 4(a) and (b) present the plasma spectra for the LIPS and SIPS systems according to particle size. A 3.3-g sample of fine dust was collected using a particle cyclone filter system and then subjected to appropriate analytical methods. Various heavy metal signals were detected simultaneously rather than in a spectrum in which only nitrogen and oxygen existed as in the gaseous state without any fine dust. A breakdown medium was observed for small

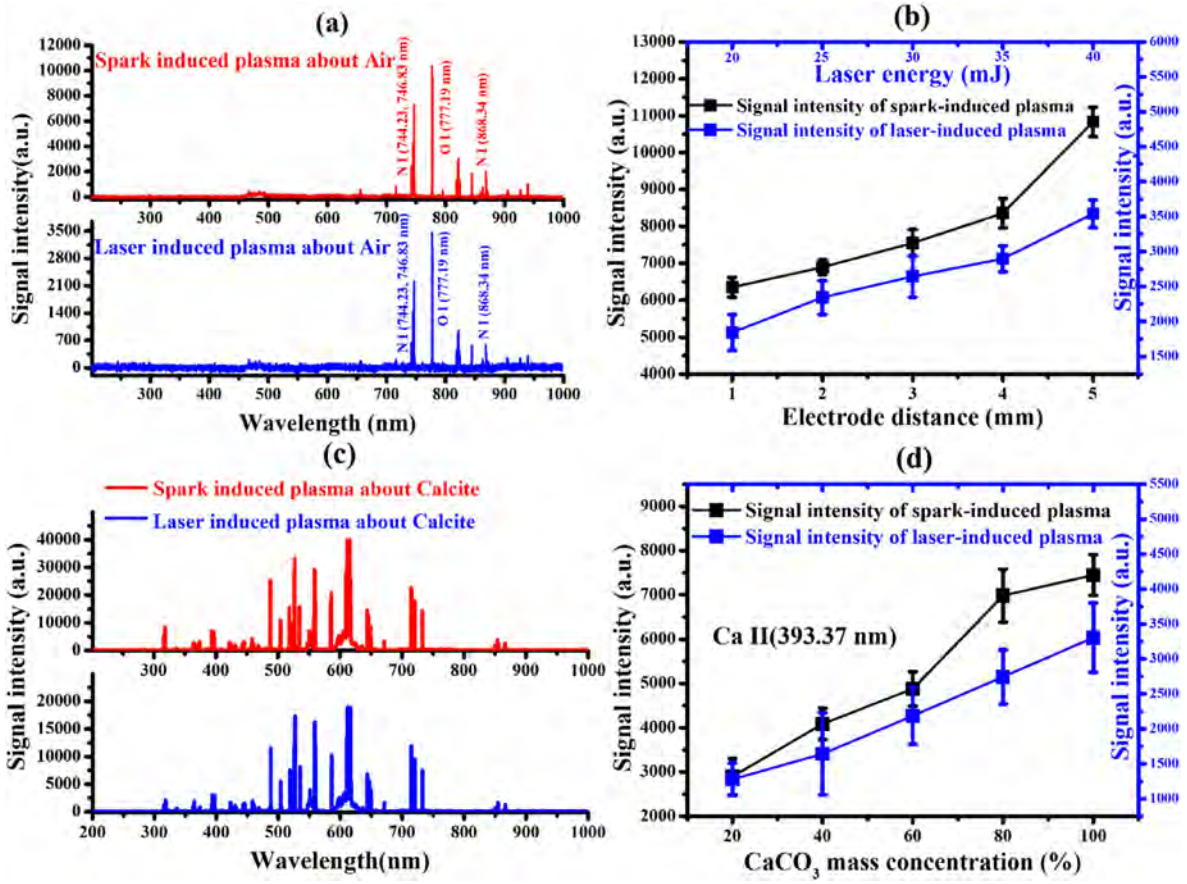

Fig. 3. For dust-free Air: (a) SIPS and LIPS results, (b) signal comparison between SIP and LIP. For Calcite: (c) SIPS and LIPS results, (d) signal comparison between SIP and LIP.

particles, indicating a high signal intensity. Additionally, when the particles were small, the breakdown of the air occurred easily and quickly.

For the fine dust sample, the plasma signal was detected within the range of 50–100 μg/m^3, as seen in Fig. 4(c) and (d). As the concentration of the fine dust increased, the signal of the heavy metals presents in the samples increased, whereas the signal strength of the wavelength for oxygen or nitrogen showed no significant changes. This meant that the signal intensity changed with varying concentrations of heavy metals and other atoms when there was a change in the fine dust concentration, and the ratio of nitrogen or oxygen atoms in the air did not vary significantly. As verification, the photodiode detection signal over various concentrations of fine dust is presented in Section 3.3.

As shown, the experiments were conducted with two different particle sizes. For both SIPS and LIPS, as the particle size increased, the signal strength decreased, thereby disrupting the breakdown medium. Also, any variations in the concentration of the fine dust particles resulted in a change in the heavy metal and other atomic signals, whereas the signals for atoms such as oxygen and nitrogen remained unchanged.

3.3. Optical configurations

Unlike the CCD camera, detection using the photodiode showed that (1) the gate width of the conventional plasma detection method was too long to detect in real-time, and (2) the optimum gate delay time was determined by identifying the integrated area of the electrical signal. As a result, determining the optimal gate delay for each heavy metal atom was advantageous for quantitative analysis. Therefore, the optimal gate delay time was derived using the values obtained from the SIPS experiments with heavy metals such as lead, iron, and copper. Herein, the electrical signals were integrated based on the delay time for manufacturing the sensing device and experimental photodiode usage. After the quantitative analysis was conducted, the following optimum gate delay times were obtained: 2.2 μs for lead, 2.6 μs for iron, 2.2 μs for copper, and 1.0 μs for NH (see Fig. S1). The optimal gate delay time for detecting the maximum signal strength at a gate width of approximately 1 μs was assumed.

Since the plasma emission of the copper signal had a signal-to-noise ratio of less than 10, it was determined that quantitative analysis was impossible in this case. For this reason, only quantitative analyses of lead and iron were conducted in this study. Here, finely powdered lead and iron samples were mixed with the dust samples circulating in the chamber before being subjected to ingredient analysis (Fig. 5). When the fine dust concentrations were varied, the lead and iron photodiode signals passing through the band-pass filter changed owing to the magnitude of the electrical signal itself. Thus, the size of the plasma itself was strongly correlated to the increase in the total concentration. However, when the fine dust concentration was kept uniform, only the lead sample showed any differences when its concentration was altered by adding lead powder. For accurate quantitative analysis, we added 0.1 μg of pure, heavy metal powder in each lead and iron sample because the minimum resolution of the microbalance (Balance XPR2U, Mettler Toledo) used was 0.1 μg. Although the strength of the electrical signal was similar here, quantitative analysis was

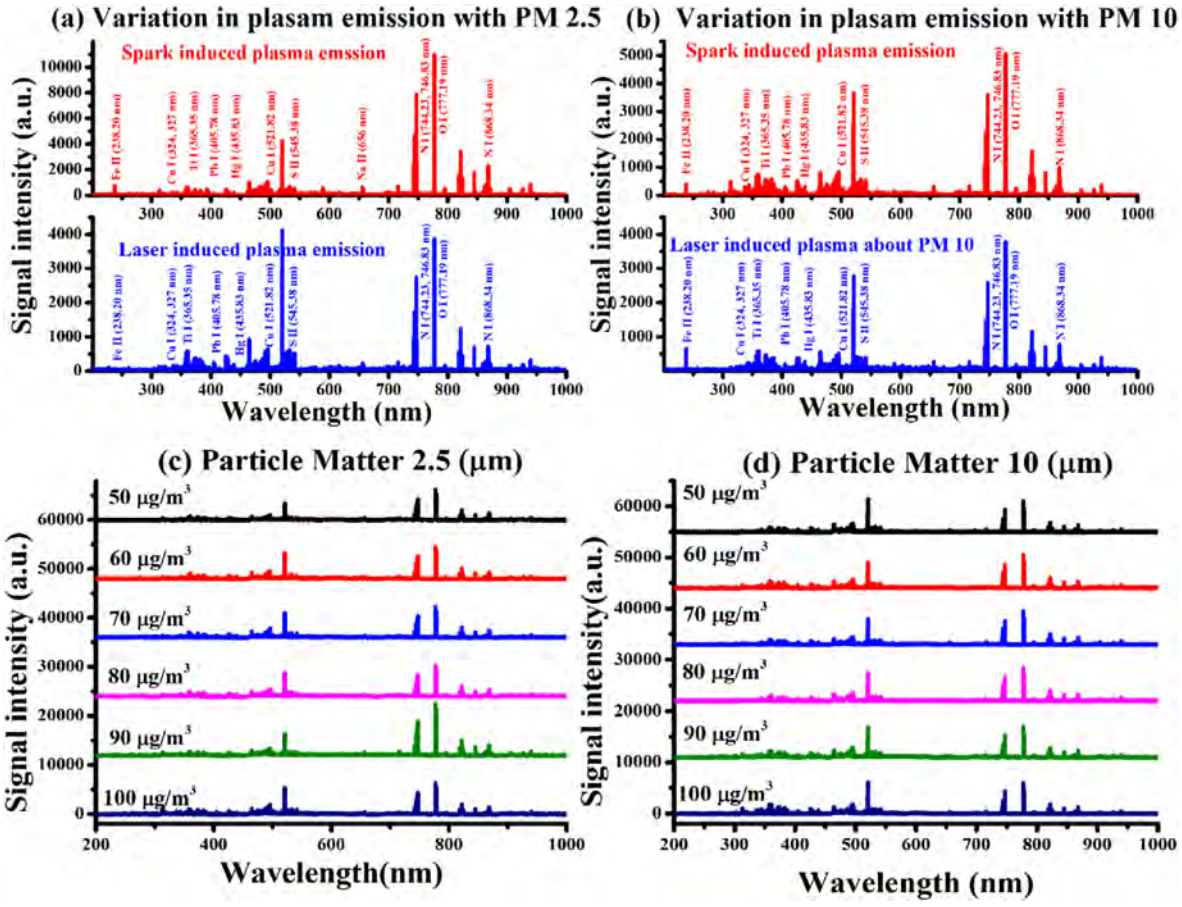

Fig. 4. Particle size effect for SIPS and LIPS: (a) PM 2.5 and (b) PM 10. Fine dust concentration effect for SIPS: (c) PM 2.5 and (d) PM 10.

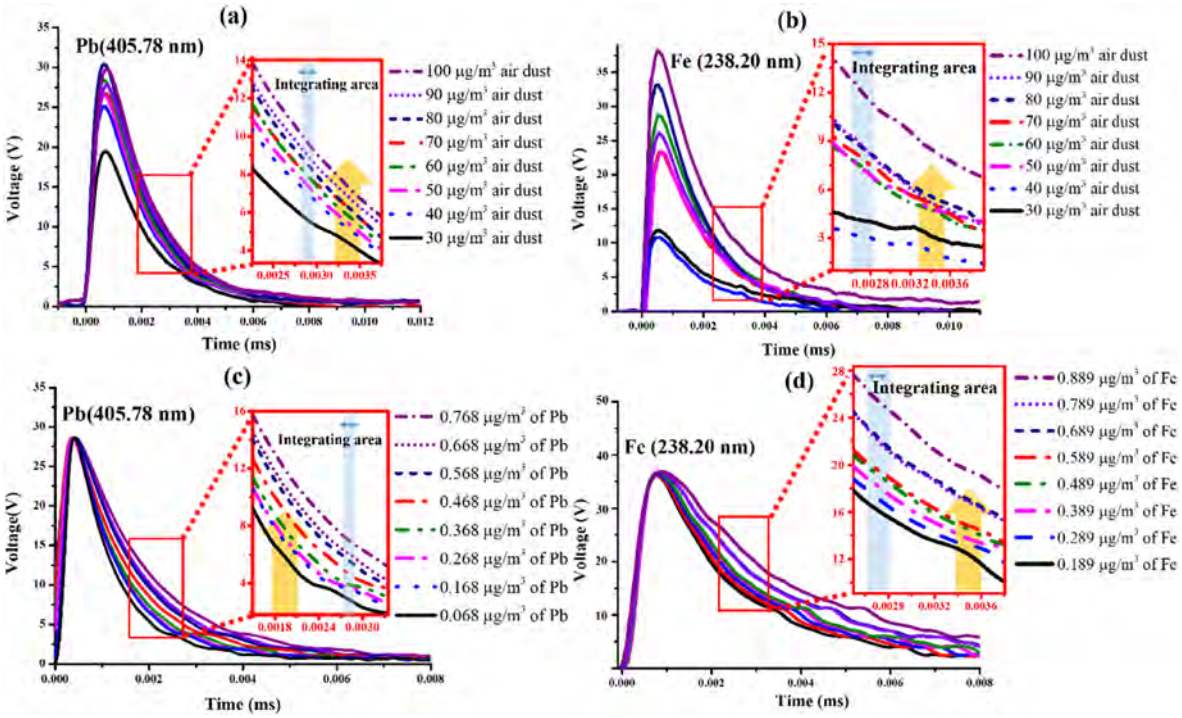

Fig. 5. Photodiode signal changes for (a) lead and (b) iron in varied concentrations of air dust. Photodiode signal changes for (c) lead and (d) iron in varied concentrations.

possible because the differences in the degree of the plasma signal decreased over time. Consequently, as the concentration of lead increased, the electrical signal exhibited a decline along the x-axis, which was expressed as the signal strength in the wavelength band, indicating Pb I (405 nm) in the plasma emission spectrum. The same situation was also observed for iron (Fig. 5(b) and (d)). When the fine dust signal changed, the plasma signal for the iron component became large, and the slope of the x-axis remained unchanged. However, when the fine dust concentration remained the same and only the iron concentration had been changed. Herein, the electrical signal intensity was the same, but the plasma signal slowly declined.

Regarding the optimal gate delay time, the integrated value could prove to be useful as a quantitative method. As presented in Fig. 6, the quantitative analysis was conducted with a very high degree of accuracy. The trends of the plasma emission spectra intensity and the electric signal integration values were similar. With these results, the proposed sensing system was determined to be a reasonable method for quantitative analysis.

3.4. Detection of ammonia

The method for detecting ammonia was devised following the protocol (Zhang et al., 2019). Herein, the NH infrared signal was 336 nm, and the signal for nitrogen was 337 nm. The photodiode system, coupled with a band-pass filter, was set to receive a band-pass filter at 5-nm intervals starting at 337 nm (see Fig. 7(a)). Thus, the sensing system detected both nitrogen and NH signals simultaneously. In this study, it was assumed that only nitrogen was detected in the pure air sample without fine dust and that quantitative analysis was conducted by comparing the electrical signals when fine dust was added while capturing the NH fluorescence signal. Even when only nitrogen was added, the reaction was possible with hydrogen in the air. Thus, the experiment was divided into two scenarios: with pure air and air containing ammonia. The pathway for producing NH ($A^3\prod.$) is shown in Equations (3)–(6) (Zhang et al., 2019; Jinkins and Wehry, 1989; Kenner et al., 1988).

$$NH_3(X) + h\nu \rightarrow NH_3(A) \quad (3)$$

$$NH_3(A) \rightarrow NH_2(X) + H \quad (4)$$

$$NH_2(X) + h\nu \rightarrow NH_2^{**} \quad (5)$$

$$NH_2^{**} \rightarrow NH(A) + H \quad (6)$$

In the presence of pure air, the electrical signal was much lower than that observed with the inflow of fine dust. Additionally, although there was an increase in the electrical signal, even in the nitrogen-only environment, the change was less than the electrical signal obtained when the fine dust containing ammonia samples were introduced. Thus, quantitative analysis of ammonia was possible with the addition of fine dust in pure air, upon removal of fine dust from the combined value of ammonium and nitrogen, and the reduction in the electrical signal caused by the concentration of pure nitrogen (see Fig. 7(b) and (c)).

4. Conclusion

A new real-time quantitative SIPS configuration was developed for detecting heavy metals and ammonia pollutants in fine dust air samples. The capability of a proposed SIPS device, suitable for controlling the frequency and magnitude of plasma, was verified by comparing the signal intensity with their counterparts obtained via the LIPS method. A novel quantitative analytical technique was additionally established by integrating time-resolved electrical signals based on the optimum delay time for each element derived.

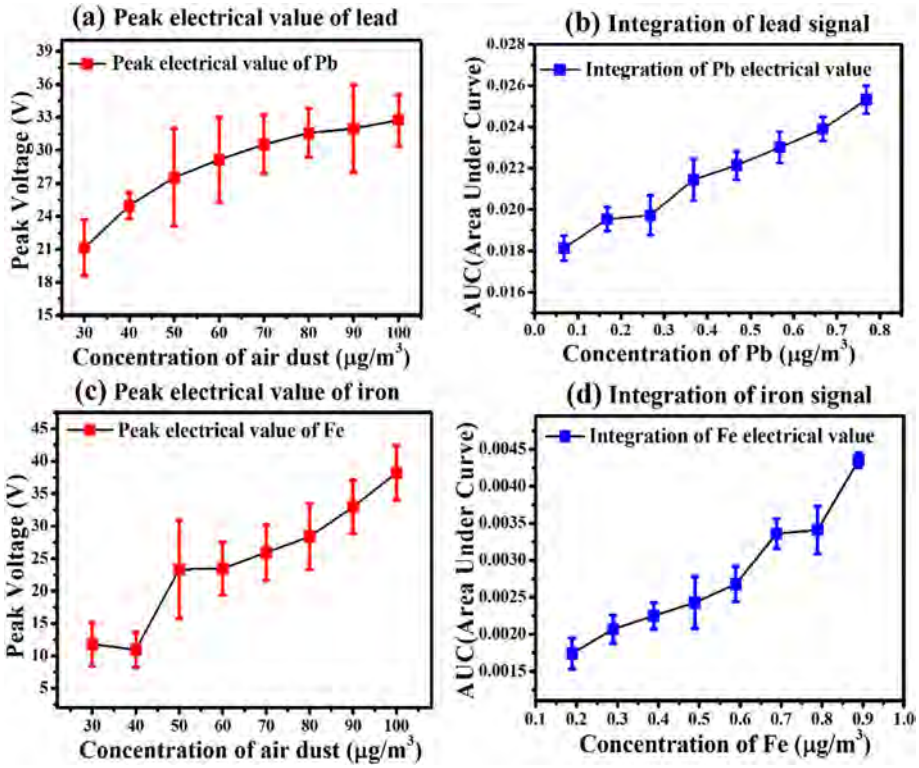

Fig. 6. For lead, (a) peak voltage signal per dust concentration and (b) its integrated signal. For iron, (c) peak voltage signal per dust concentration and (d) its integrated signal.

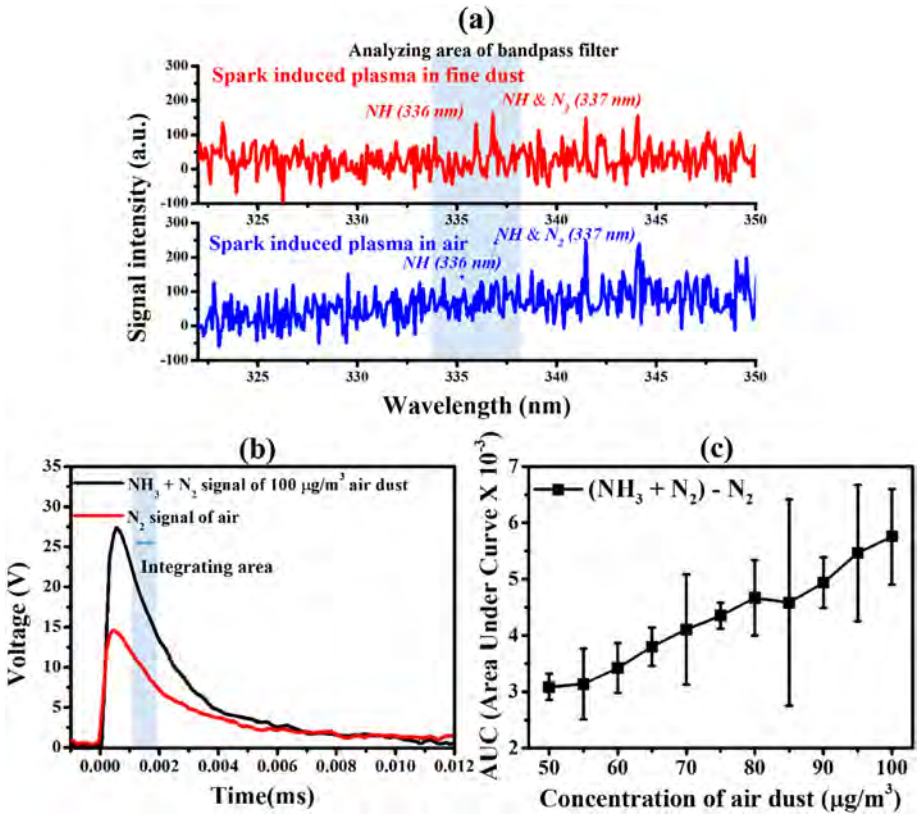

Fig. 7. (a) Ammonia signals detected in the fine dust samples, (b) voltage signals of air and dust samples, and (c) AUC per dust concentration.

Subsequently, a compact sensing device with a five-fold enhancement of LOD was built for 0.1 to 10 $\mu g/m^3$ concentrations of heavy metals and ammonia over the LIPS. The present work serves as a basis for establishing a novel atmospheric pollutant monitoring system.

Declaration of competing interest

The authors declare that they have no known competing financial interests or personal relationships that could have appeared to influence the work reported in this paper.

CRediT authorship contribution statement

Jun-Ho Yang: Formal analysis, Investigation, Writing - original draft. **Jaehun Jung:** Investigation, Writing - review & editing. **Ji-Hoon Ryu:** Investigation. **Jack J. Yoh:** Conceptualization, Formal analysis, Writing - review & editing.

Acknowledgments

This research was supported by the Basic Science Research Program through the National Research Foundation of Korea (2016R1D1A1A02937421) contracted through IAAT and IOER at Seoul National University.

Appendix A. Supplementary data

Supplementary data to this article can be found online at https://doi.org/10.1016/j.chemosphere.2020.127237.

References

Abdel-Latif, N.M., Saleh, I.A., 2012. Heavy metals contamination in roadside dust along major roads and correlation with urbanization activities in Cairo, Egypt. J. Am. Sci. 8 (6), 379–389.

Cho, H.K., Park, C.G., Shin, H.J., Park, K.H., Lim, H.B., 2018. Comparison of the in vitro toxicological activity of various particulate matter. Toxicol. Ind. Health 34 (2), 99–109. https://doi.org/10.1177/0748233717749694.

Choi, Y., Park, K., Kim, I., Kim, S.D., 2018. Combined toxic effect of airborne heavy metals on human lung cell line A549. Environ. Geochem. Health 40 (1), 271–282. https://doi.org/10.1007/s10653-016-9901-6.

Cyrys, J., Stozel, M., Heinrich, J., Kreyling, W.G., Menzel, N., Wittmaack, K., Tuch, T., Wichmann, H.-Erich, 2003. Elemental composition and sources of fine and ultrafine ambient particles in Erfurt, Germany. Sci. Total Environ. 305, 143–156. https://doi.org/10.1016/S0048-9697(02)00494-1.

Dastoorpoor, M., Idani, E., Goudarzi, G., Khanjani, N., 2018. Acute effects of air pollution on spontaneous abortion, premature delivery, and stillbirth in Ahvaz, Iran: a time-series study. Environ. Sci. Pollut. R 25 (6), 5447–5458. https://doi.org/10.1007/s11356-017-0692-9. .

Dianat, M., Radmanesh, E., Badavi, M., Goudarzi, G., Mard, S.A., 2016. The effects of PM 10 on electrocardiogram parameters, blood pressure and oxidative stress in healthy rats: the protective effects of vanillic acid. Environ. Sci. Pollut. R 23 (19), 19551–19560. https://doi.org/10.1007/s11356-016-7168-1. .

Ehrlich, C., Noll, G., Kalkoff, W.D., Baumbach, G., Dreiseidler, A., 2007. PM10, PM2. 5 and PM1. 0-emissions from industrial plants-results from measurement programmes in Germany, Atmos. Environ. Times 41 (29), 6236–6254. https://doi.org/10.1016/j.atmosenv.2007.03.059.

Guo, Z.G., Feng, J.L., Fang, M., Chen, H.Y., Lau, K.H., 2002. The elemental and organic characteristics of PM2.5 in Asian dust episodes in Qingdao, China, 2002. Atmos. Environ. 38 (6), 909–919. https://doi.org/10.1016/j.atmosenv.2003.10.034.

Hadei, M., Naddafi, K., 2020. Cardiovascular effects of airborne particulate matter: a review of rodent model studies. Chemosphere 242, 125–204. https://doi.org/10.1016/j.chemosphere.2019.125204. .

Hagen, L.J., 2004. Fine Particulates (PM10 and PM2.5) generated bt breakage of mobile aggregates during simulated wind erosion. Trans. ASAE (Am. Soc. Agric. Eng.) 47 (1), 107–112. https://doi.org/10.13031/2013.15876.

He, X., Dong, B., Chen, Y., Li, R., Wang, F., Li, J., Cai, Z., 2018. Analysis of magnesium and copper in aluminum alloys with high repetition rate laser-ablation spark-induced breakdown spectroscopy. Spectrochim. Acta, Part B 141, 34–43. https://doi.org/10.1016/j.sab.2018.01.007.

Hunter, A.J.R., Davis, S.J., Piper, L.G., Holtzclaw, K.W., Fraser, M.E., 2000b. Spark-

induced breakdown spectroscopy: a new technique for monitoring heavy metals. Appl. Spectrosc. 54 (4), 575–582. https://doi.org/10.1366/0003702001949753.

Hunter, A.J., Morency, J.R., Senior, C.L., Davis, S.J., Fraser, M.E., 2000a. Continuous emissions monitoring using spark-induced breakdown spectroscopy. J. Air Waste Manag. Assoc. 50 (1), 111–117. https://doi.org/10.1080/10473289.2000.10463982.

Jinkins, J.G., Wehry, E.L., 1989. Laser photolytic fragmentation fluorescence spectrometry of ammonia and aliphatic amines. Appl. Spectrosc. 43, 861–865. https://doi.org/10.1366/0003702894202193.

Jun, H., Kim, J.H., Lee, S., Yoh, J.J., 2018. Towards simplified monitoring of instantaneous fuel concentration in both liquid and gas fueled flames using a combustor injectable LIBS plug. Energy 160, 225–232. https://doi.org/10.1016/j.energy.2018.07.016.

Jung, J., Yang, J. -H., Yoh, 2020. An optimal configuration for spark-induced breakdown spectroscopy of bulk minerals aimed at planetary analysis. J. Anal. Atom. Spectrosc. https://doi.org/10.1039/D0JA00057D.

Kammermann, T., Kreutner, W., Trottmann, M., Merotto, L., Soltic, P., Bleiner, D., 2018. Spark-induced breakdown spectroscopy of methane/air and hydrogen-enriched methane/air mixtures at engine relevant conditions. Spectrochim. Acta, Part B 148, 152–164. https://doi.org/10.1016/j.sab.2018.06.013.

Kenner, R.D., Browarzik, R.K., Stuhl, F., 1988. Two-photon formation of NH.ND($A^3\pi$) in the 193 nm photolysis of ammonia. II. Photolysis of NH_2. Chem. Phys. 121, 457–471. https://doi.org/10.1016/0301-0104(87)85043-7.

Khalaji, M., Roshanzadeh, B., Mansoori, A., Taefi, N., Tavassoli, S.H., 2012. Continuous dust monitoring and analysis by spark induced breakdown spectroscopy. Optic Laser. Eng. 50 (2), 110–113. https://doi.org/10.1016/j.optlaseng.2011.10.009.

Lelieveld, J., Evans, J.S., Fnais, M., Giannadaki, D., Pozzer, A., 2015. The contribution of outdoor air pollution sources to premature mortality on a global scale. Nature 525 (7569), 367–371. https://doi.org/10.1038/nature15371.

Neisi, A., Vosoughi, M., Idani, E., Goudarzi, G., Takdastan, A., Babaei, A.A., Hazrati, S., Shoshtari, M.H., Mirr, I., Maleki, H., 2017. Comparison of normal and dusty day impacts on fractional exhaled nitric oxide and lung function in healthy children in Ahvaz, Iran. Environ. Sci. Pollut. R 24 (13), 12360–12371. https://doi.org/10.1007/s11356-017-8853-4. .

Ng, S., Chan, L., Lam, K., Chan, W., 2003. Heavy metal contents and magnetic properties of playground dust in Hong Kong. Environ. Monit. Assess. 89, 221–232. https://doi.org/10.1023/A:1026103318778.

Park, M., Joo, H.S., Lee, K., Jang, M., Kim, S.D., Kim, I., Borlaza, L.J.S., Lim, H., Shin, H., Chung, K.H., Choi, Y.H., Park, S.G., Bae, M.S., Lee, J., Song, H., Park, K., 2018. Differential toxicities of fine particulate matters from various sources. Sci. Rep. 8 (1), 17007. https://doi.org/10.1038/s41598-018-35398-0.

Prospero, J.M., Olmez, I., Ames, M., 2001. Al and Fe in PM 2.5 and PM 10 suspended particles in south-central Florida: the impact of the long range transport of African mineral dust. Water Air Soil Pollut. 125 (1), 291–317. https://doi.org/10.1023/A:1005277214288.

Srungaram, P.K., Ayyalasomayajula, K.K., Yu-Yueh, F., Singh, J.P., 2013. Comparison of laser induced breakdown spectroscopy and spark induced breakdown spectroscopy for determination of mercury in soils. Spectrochim. Acta, Part B 87, 108–113. https://doi.org/10.1016/j.sab.2013.05.009.

Stone, E.A., Yoon, S.C., Schauer, J.J., 2011. Chemical characterization of fine and coarse particles in Gosan, Korea during springtime dust events. Aerosol Air Qual. Res. 11 (1), 31–43. https://doi.org/10.4209/aaqr.2010.08.0069.

Sugimoto, N., Uno, I., Nishikawa, M., Shimizu, A., Matsui, I., Dong, X., Chen, Y., Quan, H., 2003. Record heavy Asian dust in Beijing in 2002: observations and model analysis of recent events. Geophys. Res. Lett. 30, 1640. https://doi.org/10.1029/2002GL016349.

VanCuren, R.A., Cahill, T.A., 2002. Asian aerosols in North America: frequency and concentration of fine dust. J. Geophys. Res. 107 https://doi.org/10.1029/2002JD002204. AAC-19.

Vieira, A.L., Silva, T.V., Sousa, F.S.I., Senesi, G.S., Santos Junior, D., Ferreira, E.C., Neto, J.A.G., 2018. Determinations of phosphorus in fertilizers by spark discharge-assisted laser-induced breakdown spectroscopy. Microchem. J. 139, 322–326. https://doi.org/10.1016/j.microc.2018.03.011.

Winchester, J.W., 1981. Fine and coarse aerosol composition from a rural area in North China. Atmos. Environ 15 (6), 933–937. https://doi.org/10.1016/0004-6981(81)90093-7.

Yao, S., Xu, J., Zhang, X., Zhang, L., Lu, Z., Lu, J., 2018. Real-time measurement of constituents in solid materials using particle flow spark induced breakdown spectroscopy. J. Anal. At. Spectrom. 33 (6), 986–991. https://doi.org/10.1039/C8JA00075A.

Yu, X., Zhu, B., Yin, Y., Yang, J., Li, Y., Bu, X., 2011. A comparative analysis of aerosol properties in dust and haze-fog days in a Chinese urban region. Atmos. Res. 99, 241–247. https://doi.org/10.1016/j.atmosres.2010.10.015.

Zhang, D., Gao, Q., Li, B., Liu, J., Li, Z., 2019. Ammonia measurements with femtosecond laser-induced plasma spectroscopy. Appl. Optic. 58 (5), 1210–1214. https://doi.org/10.1364/AO.58.001210.

Zhang, L., Kok, J.F., Henze, D.K., Li, Q., Zhao, C., 2013b. Improving simulations of fine dust surface concentrations over the western United States by optimizing the particle size distribution. Geophys. Res. Lett. 40, 3270–3275. https://doi.org/10.1002/grl.50591.

Zhang, H., Luo, Y., Makino, T., Wu, L., Nanzyo, M., 2013a. The heavy metal partition in size-fractions of the fine particles in agricultural soils contaminated by waste water and smelter dust. J. Hazard Mater. 248, 303–312. https://doi.org/10.1016/j.jhazmat.2013.01.019.